IEEE Access
Multidisciplinary | Rapid Review | Open Access Journal

Received March 12, 2019, accepted April 6, 2019, date of current version May 6, 2019.

Digital Object Identifier 10.1109/ACCESS.2019.2913153

PWM Modulation and Control Strategy for LLC-DCX Converter to Achieve Bidirectional Power Flow in Facing With Resonant Parameters Variation

JINGTAO XU[1,2], JIAN YANG[1,2], (Member, IEEE), GUO XU[1,2], (Member, IEEE), TAOWEN JIANG[1,2], MEI SU[1,2], YAO SUN[1,2], (Member, IEEE), HUI WANG[1,2], AND MINGHUI ZHENG[3]

[1]School of Automation, Central South University, Changsha 410083, China
[2]Hunan Provincial Key Laboratory of Power Electronics Equipment and Grid, Changsha 410083, China
[3]Department of Mechanical and Aerospace Engineering, University at Buffalo, Buffalo, NY 14260, USA

Corresponding author: Guo Xu (xuguocsu@csu.edu.cn)

This work was supported in part by the National Key R&D Program of China under Grant 2018YFB0606005, in part by the National Natural Science Foundation of China under Grant 61573384, in part by the Key Technology R&D Program of Hunan Province of China under Grant 2018SK2140, and in part by the Fundamental Research Funds in the Central South University under Grant 2018zzts529.

ABSTRACT The LLC resonant converter can be used as a dc–dc transformer (DCX) to provide isolation and fixed voltage transfer ratio. For applications requiring bidirectional power transmission, this paper proposes a PWM modulation and control strategy to achieve naturally bidirectional power flow for LLC-DCX, even in the case when the resonant parameters vary. Without the loss of generality, the proposed modulation can achieve ZVS of one side switches and ZCS of other side switches. Meanwhile, the additional benefits are that the PWM logic exchanging of the primary full bridge and the secondary full bridge is avoided and the auxiliary SR circuit is not needed. This simplifies the control and makes the converter to achieve naturally bidirectional power flow. Meanwhile, according to the analysis, it can also provide a fixed voltage conversion ratio independent of switching frequency if properly designed. Furthermore, to accurately locate the zero-crossing instant of the current when resonant parameters vary, the optimal duty cycle tracking based on the perturbation and observation method (P&O) is adopted. The characteristics and design considerations of the proposed modulation and control are also presented in detail in this paper. Finally, the experimental results are given to verify the effectiveness and advantages of the proposed solution.

INDEX TERMS Bidirectional power flow, DCX, fixed voltage gain, LLC converter, optimal duty cycle tracking.

I. INTRODUCTION

IN recent years, isolated bidirectional DC/DC converters (BDCs) are developing rapidly which have been widely used in electric vehicles, uninterruptible power supplies, and energy storage systems. In view of the power topology for these applications, one solution being adopted by [1]–[3] is dual active-bridge (DAB) converter. It has advantages such as symmetrical structure, ZVS capability, naturally bidirectional power flow control [4]. However, it suffers from limited ZVS range and high turn-off current, leading to a decreased power conversion efficiency. Even though the performance can be improved with other modulation strategy [5]–[7], the control complexity is increased.

In view of the efficiency, LLC resonant converter is another attractive topology because of its soft-switching characteristics for all power devices under zero to full load range [8]–[13]. When conversion gain range is narrow, such as operating at the resonant frequency, it has very high conversion efficiency as ZVS turn-on and ZCS turn-off can be achieved. While, if the conversion gain needs to be widely adjusted, the converter operating frequency has to be away from the resonant frequency, which could generate high circulating current and reduce the efficiency greatly [14].

The associate editor coordinating the review of this manuscript and approving it for publication was Yijie Wang.

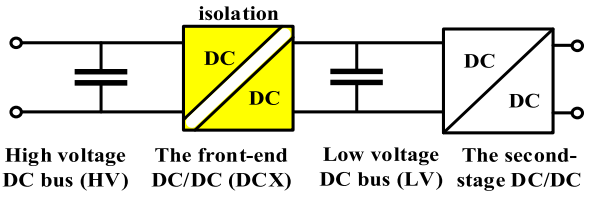

FIGURE 1. Two-stage scheme.

To address the issue under wide conversion gain range, two stage conversion structure is studied in [15]–[17] as shown in Fig.1. The front-end is a LLC resonant converter operating near the resonant frequency to achieve the isolation with high conversion efficiency and it without voltage controller. The voltage regulation capability and the dynamic performance are provided by the second-stage converters, so the second-stage is usually a non-isolated bidirectional DC-DC converter (e.g. synchronous rectifier Buck converter) to achieve the voltage gain adjustment. The LLC converter for the front-end converter of two-stage solution is named as DC/DC transformer (LLC-DCX) [18], because the operating frequency is fixed and the conversion gain is unregulated.

For the two-stage solution employing LLC-DCX, most of studies are focused on the unidirectional power applications [19], [20]. Under unidirectional power transmission, the primary side full bridge acts as a high frequency inverter, and the secondary side full bridge acts as a synchronous rectifier (SR). The realization of synchronous rectification needs to control the duty cycle of secondary switches accurately. Some methods detect the current zero crossing point [21] or drain-source voltage of switches [22], [23], but additional sensors complicate the topology and it increase the cost. Besides, the performance is affected by parasitic parameters of the circuit. [24] and [25] predict the optimal duty cycle by mathematical model, but in practice, the accuracy of implementation is low. In addition, the coupling of switching frequency, secondary duty cycle and voltage gain will lead to the complexity of control algorithm.

These methods of synchronous rectification make the driver logic different for the two full bridges, and the equivalent model of resonant tank is asymmetric under bidirectional power transmission. To achieve the symmetry of the resonant tank under bidirectional power transmission for LLC converter, an auxiliary inductor is added in [26], and an auxiliary capacitor can also be added to a CLLC converter [27]. While SR are both need, hence it still cannot be switched smoothly under bidirectional power application. In addition, the power transfer mode exchanging requires the high accuracy sampling, which increases the complexity of the control. In [28], [29], the driving signals of the primary side and secondary side are identical under fixed conversion gain. However, the turn off instant of the switches need to be controlled at the point when the leakage inductor current and magnetizing current is crossing. This is hard to control in practice, because resonant parameters may change due to magnetics manufactory, aging and parametric inconsistency. To address this problem, some observation-based control strategies are proposed [30], [31]. In [30] the harmonics approximation modeling approach is presented, and the pulse width locked loop is used in [31]. However, these methods are to track and adjust the resonant frequency. The existence of the switching dead time and the coupling between the switching frequency and voltage gain will increase the difficulty of implementation.

In order to achieve natural bidirectional power flow and easy of control, a modulation and control strategy is proposed in this paper which has the following advantages:

1) In the proposed modulation, the resonant current is completely discontinuous with proper design and the magnetizing inductance does not participate in the resonance which is only used to achieve soft-switching. Under this circumstance, constant voltage gain can be achieved under different operating frequency regardless of the load.
2) The driving signals of the primary and secondary sides are identical in bidirectional power transmission. Hence the LLC operating in the proposed modulation is a natural bidirectional topology. This greatly reduces the control complexity of the bidirectional system. Without the judgment and switching of the mode, the reliability of the system will be improved.
3) When the resonant parameters change, the converter can locate the zero-crossing point accurately and provide the fixed voltage ratio by proposed optimal duty cycle tracking method. Compared with [24], [25] and [31], the LLC converter works at a fixed switching frequency which is less than the resonant frequency in this paper, and the switching frequency and voltage gain are decoupled. Therefore, the logic of the proposed control strategy is concise. Compared with [21]–[23], its realization only depends on the input and output voltage sampling without any auxiliary circuit.

In this paper, a modulation and control strategy are proposed to achieve natural bidirectional power flow. The problems of conventional LLC under bidirectional power flow are presented in Section II. In order to solve these problems, the proposed modulation is presented and analyzed in Section III. Based on that, to accurately locate the zero-crossing point under the change of resonant parameters, an optimal duty cycle tracking by perturbation and observation method (P&O) is presented in Section IV. The design considerations are given in Section V. Experimental results based on a prototype are shown in Section VI, which verifies the effectiveness of the proposed solution.

II. PROBLEMS OF CONVENTIONAL LLC UNDER BIDIRECTIONAL POWER FLOW

The LLC resonant converter topology is shown in Fig.2. The converter is composed of two active full bridges, a transformer and a LLC network. V_{HV} stands for the high side voltage, and V_{LV} is the low side voltage. It is defined that the forward power operation occurs when power transfers from

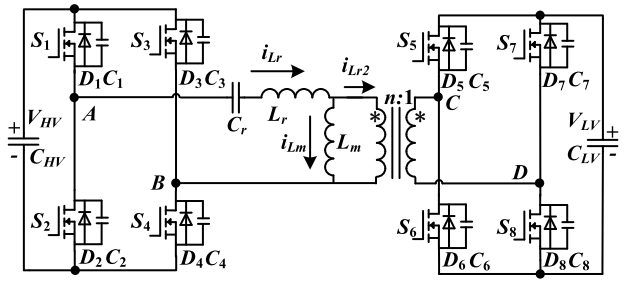

FIGURE 2. LLC resonant converter.

high voltage side to the low voltage side, otherwise the converter runs at backward operation. Under normal operation, one full bridge works as a high frequency voltage inverter, and the other side full bridge works as a SR. Generally, to achieve the ZVS of one side switches and ZCS of the other side switches, it is suggested to operate the switching frequency f_s to be higher than the resonant frequency of the resonant tank f_r [32] which is shown as

$$f_s > f_r = \frac{1}{2\pi\sqrt{L_r C_r}} \tag{1}$$

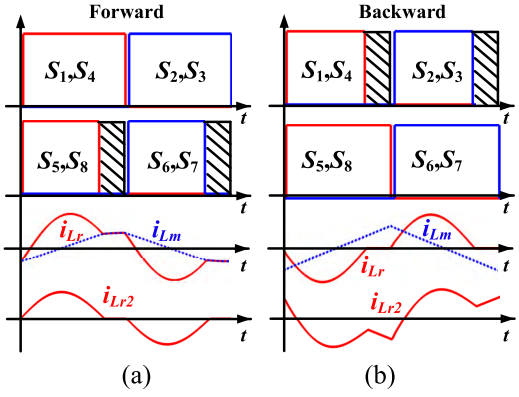

FIGURE 3. Traditional LLC key waveforms. (a) Forward operation, (b) Backward operation.

The theoretical waveforms when $f_s > f_r$ under forward and backward power transmission are shown in Fig.3. Under forward operation, as shown in Fig.3(a), the turn on time for S_5 & S_8 (or S_6 & S_7) is shorter than S_1 & S_4 (or S_2 & S_3) to achieve exactly ZCS of switches and also to avoid backward resonance [33]. While, under backward operation, as shown in Fig.3(b), the turn on time for S_5 & S_8 (or S_6 & S_7) is longer than S_1 & S_4 (or S_2 & S_3).

When the power directions changes, the roles for the two full bridges will exchange, and the driving signals for the two full bridges needs to be exchanged accordingly [34]. This mode exchanging requires the high accurate sampling of the voltage and current to evaluate the power, and it also increases the complexity of the control. Besides, when the LLC is under backward operation, the excitation inductance is clamped all the period, which results in the change of the voltage gain characteristics. Therefore, the traditional LLC resonant converter is not a natural bidirectional power flow topology. Furthermore, the accurate achieving of synchronous rectification requires additional auxiliary circuits to locate zero crossing point of resonant current [35]. In bidirectional power applications, if these circuits are added, all the eight switches PWM signals have to change the role between zero cross detection mode and inverting mode according to the power direction. This would increase the complexity of both the hardware and software design.

To avoid the aforementioned undesired situations, one way is to make the turn-on time for all the switches exactly the same. Then, the exchanging of inverter mode and rectifying mode is not necessary. This requires the converter to working exactly at the point when switching frequency ($f_s = f_r$), which serves as an isolated converter with constant voltage gain (LLC-DCX) [31]. The DCX working point in the voltage gain curve$M(f_N)$ of LLC converter under different Q (Quality Factor) are shown in Fig.4. Where $f_N = f_s/f_r$ and $M(f_N) = nV_{LV}/V_{HV}$. n is the transformer ratio.

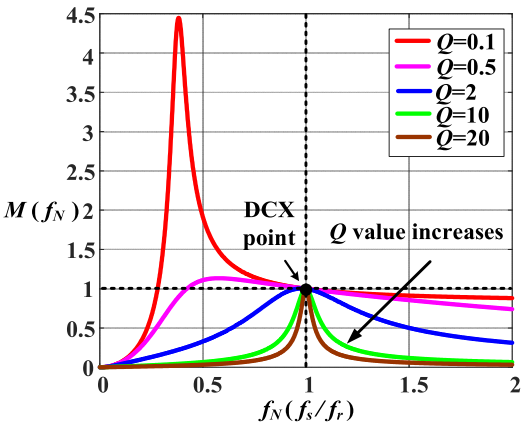

FIGURE 4. Voltage Gain curves of LLC.

As shown in Fig.4, theoretically, when operated at DCX point, the voltage gain will be constant. However, in practice, because the parameters of resonant components can vary due to magnetics manufactory, aging and parametric inconsistency, the operating frequency will change to the two sides of the DCX point. Once the DCX point are not ensured, PWM logic exchanging will still be needed to avoid backward resonance, and the fixed gain property is lost because the voltage gain will change as seen from Fig.4.

III. PROPOSED MODULATION TO ACHIEVE NATURAL BIDIRECTIONAL POWER

A. OPERATION MODES UNDER PROPOSED MODIFIED MODULATION STRATEGY

In this section, a modified modulation strategy is presented. It can provide fixed voltage ratio, natural bidirectional power flow, and synchronous secondary rectification without adding auxiliary circuit.

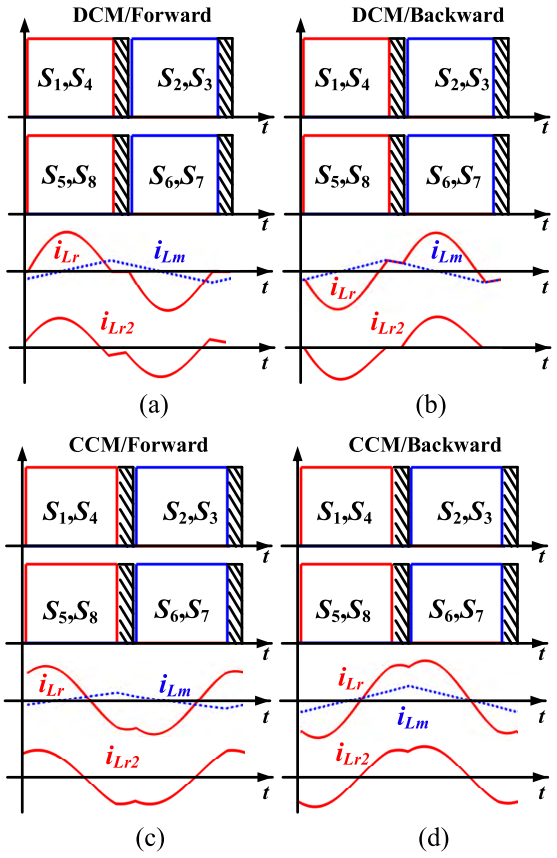

FIGURE 5. Key waveforms of the proposed Modulation. (a) Forward operation of DCM, (b) Backward operation of DCM, (c) Forward operation of CCM, (d) Backward operation of CCM.

The key waveforms of the proposed modulation are illustrated in Fig.5. The difference of the proposed modulation strategy in comparison with the traditional LLC resonant converter is that the switches of the HV side and the LV side work simultaneously. The switching frequency is fixed and less than the resonant frequency. It only needs to ensure that their duty cycle is equal to the half resonant period as shown in (2).

$$D = T_r/2T_s \tag{2}$$

where T_s and T_r are the switching period and the resonant period. D is the duty cycle of switches.

As shown in Fig.5, there are two operating modes with the proposed modulation: discontinuous current mode (DCM) and current continuous mode (CCM). When the converter operates in CCM, the circulating current and turn-off loss will increase. Besides, the zero-crossing point of the resonant current changes with load, which results in that the voltage ratio is no longer fixed. Hence CCM should be avoided in practice. As a result, only DCM operation are discussed here, and the design to avoid CCM operation would be given in later Part C.

Under DCM, once (2) is satisfied, the voltage ratio is independent of switching frequency. Meanwhile, the magnetizing inductance does not participate in resonance all the period. Since the forward and reverse modes are symmetrical, only forward operation is analyzed. The detailed working waveforms of forward operation is shown in Fig.6.

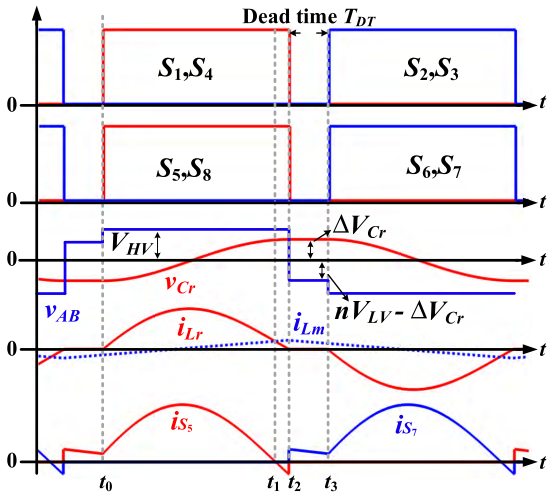

FIGURE 6. Detailed working waveforms of the forward operation.

Before t_0, all switches are turned off. v_{Cr} is at its minimum value -ΔV_{Cr}. The resonant current i_{Lr} is intermittent. The excitation current i_{Lm} flows through D_5 and D_8 to LV output terminal V_{LV}. As shown in the Fig. 7(a).

Stage 1 [t_0, t_1] [see Fig. 7(b)]: At t_0, S_1, S_4, S_5 and S_8 are turned on, where S_5 and S_8 are turned on with ZVS. The resonant inductor current i_{Lr} of the HV side can be expressed as

$$i_{Lr}(t) = \frac{V_{HV} - nV_{LV} + \Delta V_{Cr}}{Z_r} \sin w_r(t - t_0) \tag{3}$$

where $Z_r = \sqrt{L_r/C_r}$, and $\omega_r = 2\pi f_r$. ΔV_{Cr} is the peak value of resonant capacitor voltage.

The relationship between i_{Lm}, i_{Lr} and i_{Lr2} is expressed as

$$i_{Lr2} = i_{Lr} - i_{Lm} \tag{4}$$

The secondary-winding of the transformer is clamped by V_{LV}. Hence i_{Lm} is expressed as

$$i_{Lm}(t) = -i_{L_m}(t_0) + \frac{nV_{LV}}{L_m}(t - t_0) \tag{5}$$

Stage 2 [t_1, t_2] [see Fig. 7(c)]: At t_1, i_{Lr} is equal to i_{Lm}. This time is different from the traditional LLC resonant converter. S_5 and S_8 are still on at this time. The excitation inductor L_m is still clamped by the second side voltage. Thus, L_m is not involved in resonance.

The relationship between i_{Lm}, i_{Lr} and i_{Lr2} is expressed as

$$i_{L_m} = i_{L_r} + i_{Lr2} \tag{6}$$

where I_{Lr2} is reversed.

At t_2, the resonant current is reduced to zero. S_1, S_4, S_5 and S_8 are turned off, where S_1 and S_4 are turned off with ZCS.

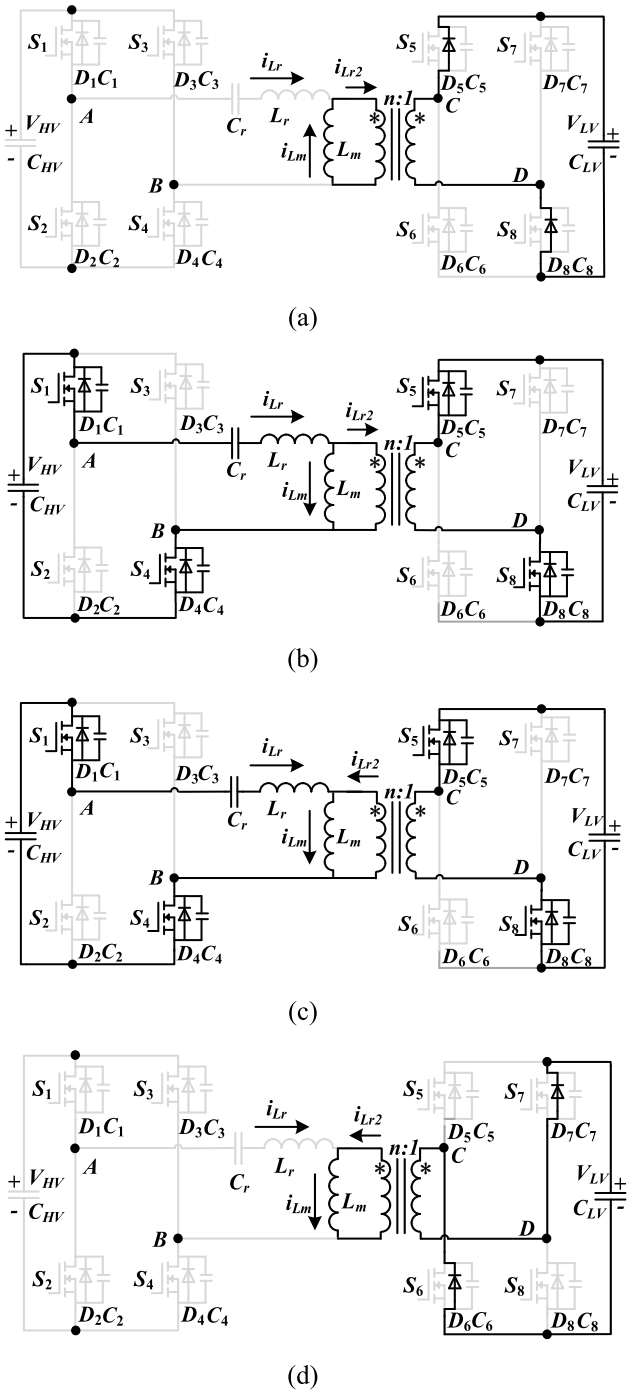

FIGURE 7. Equivalent circuit of (a) Before t_0, (b) $[t_0, t_1]$, (c) $[t_1, t_2]$, (d) $[t_2, t_3]$.

Stage 3 $[t_2, t_3]$ [see Fig. 7(d)]: During this period, i_{Lr} is zero and v_{Cr} remains in ΔV_{Cr}. The excitation current flow through D_6, D_7.

After t_3, the operation mode is similar to stage 1, and the other half switching period begins.

In the half period, the relationship between v_{Cr} and i_{Lr} is expressed as

$$C_r \frac{dv_{Cr}}{dt} = i_{Lr}(t) \tag{7}$$

v_{Cr} is from -ΔV_{Cr} to ΔV_{Cr} by 1/2 switching periods, hence ΔV_{Cr} is expressed as

$$\Delta V_{Cr} = \frac{\int_0^{T_s/2} i_{Lr}(t) \cdot dt}{2C_r} = \frac{P}{4V_{HV} f_s C_r} \tag{8}$$

where P is the transmission power.

B. CONSTANT VOLTAGE GAIN

The average value of the resonant current $i_{Lr}(t)$ is equal to I_{HV} which can be obtained by

$$\begin{aligned} I_{HV} &= 2f_s \int_{t_0}^{t_2} i_{Lr}(t) \cdot dt \\ \Rightarrow I_{HV} &= 4f_s \frac{V_{HV} - nV_{LV} + \Delta V_{Cr}}{Z_r \omega_r} \end{aligned} \tag{9}$$

Ignoring the power losses, the HV side current can also be expressed as

$$I_{HV} = V_{LV}^2 / (V_{HV} R_{LV}) \tag{10}$$

where R_{LV} is the equivalent resistance of V_{LV}.

Substitute (8) and (9) into (10), the relationship between the V_{HV} and V_{LV} can be derived

$$\begin{aligned} 4f_s \frac{V_{HV} - nV_{LV} + \Delta V_{Cr}}{Z_r \omega_r} &= \frac{V_{LV}^2}{V_{HV} R_{LV}} \\ \Rightarrow V_{HV} - nV_{LV} &= \frac{V_{LV}^2 Z_r \omega_r}{4f_s V_{HV} R_{LV}} - \Delta V_{Cr} \\ \Rightarrow V_{HV} - nV_{LV} &= \frac{V_{LV}^2}{V_{HV} R_{LV}} \left(\frac{Z_r \omega_r}{4f_s} - \frac{1}{4f_s C_r} \right) = 0 \\ \Rightarrow V_{HV} &= nV_{LV} \end{aligned} \tag{11}$$

According to (11), the voltage gain curves can be obtained as shown in Fig.8. When $f_s < f_r$, the voltage transfer ratio of the proposed modulation is kept constant to 1 which is load-independent.

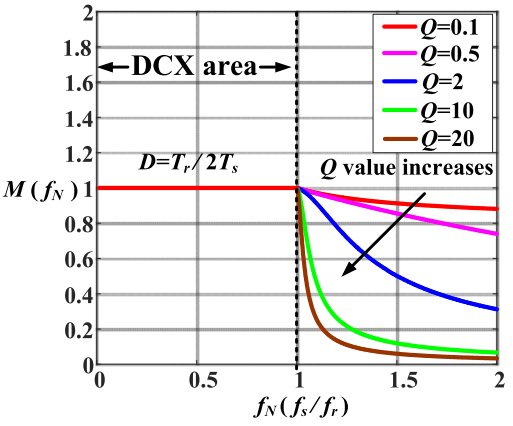

FIGURE 8. Voltage Gain curves of the proposed modulation.

C. CONDITIONS OF DCM OPERATION

At t_2, i_{Lr} is zero while v_{Cr} is ΔV_{Cr} as shown in Fig.6. For the resonant tank, the resonant capacitor tends to discharge, while the resonant current i_{Lr} trends to reverse backward. As shown in Fig.9(a), assuming that the resonant current is reversed, the resonant current of HV side will flow through D_1, D_4, and the resonant current of LV side will flow through D_6, D_7. In this case, the converter operates in CCM.

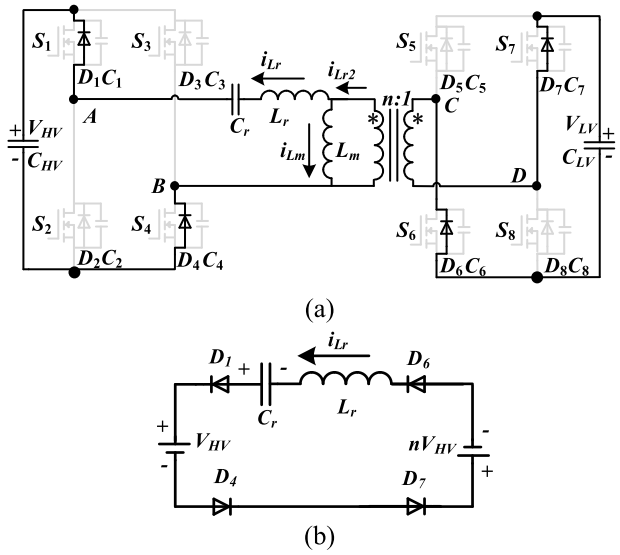

FIGURE 9. Converter works in CCM (a) Equivalent circuit, (b) Simplified resonant tank.

The simplified resonant tank is shown in Fig.9(b). Ignoring the forward voltage drop of the diodes, then the conduction condition of the four diodes is expressed as

$$\Delta V_{C_r} - (V_{HV} + nV_{LV}) - L\frac{di_{Lr}}{dt} > 0 \tag{12}$$

where i_{Lr} is expressed as

$$i_{Lr}(t) = \frac{-(V_{HV} + nV_{LV}) + \Delta V_{Cr}}{Z_r} \sin w_r(t - t_0) \tag{13}$$

Assuming that the resonant current is critical continuous, then $\Delta V_{Cr} - (V_{HV}+nV_{LV})$ is approximately equal to zero. Hence the resonant inductance voltage $L{\cdot}di_{Lr}/dt$ can be ignored. According (12), the conduction condition is expressed as

$$\begin{aligned} &\Delta V_{Cr} - (V_{HV} + nV_{LV}) > 0 \\ &\Rightarrow \frac{P}{4V_{HV}f_sC_r} - 2V_{HV} > 0 \\ &\Rightarrow P > 8V_{HV}^2 f_s C_r \end{aligned} \tag{14}$$

Equation (14) shows that, when $P < 8V_{HV}^2 f_s C_r$ is satisfied, all the diodes are reverse biased and hence there is no possibility for the oscillation to continue by reversing the current direction which means the converter operates in DCM mode. The boundary condition of DCM and CCM is shown in Fig.10. When the input voltage and switching frequency of the converter are determined, the resonant capacitance is proportional to the critical power of DCM.

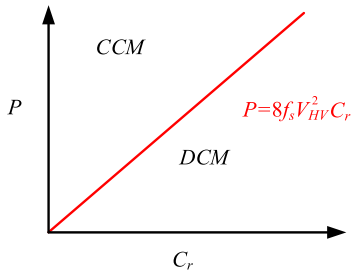

FIGURE 10. Boundary conditions of DCM and CCM.

IV. OPTIMAL DUTY CYCLE TRACKING BY PERTURBATION AND OBSERVATION METHOD (P&O)

The waveforms of i_{Lr} with mismatched resonant period and duty cycle D are shown in Fig.11.

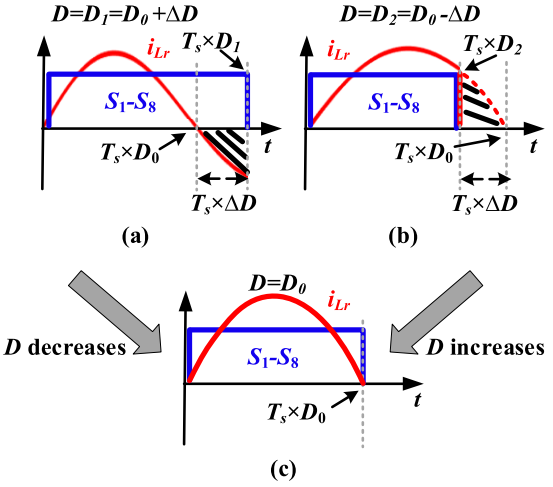

FIGURE 11. Waveforms under the different duty cycle. (a) $D_1 = D_0 + \Delta D$, (b) $D_2 = D_0 - \Delta D$, (c)$D = D_0$.

The average value of LV side current in the three cases can be expressed as

$$\begin{cases} I_{LV1} = 2\dfrac{n}{T_s}\int_0^{T_s\times D_1} i_{Lr}(t)\cdot dt \\ = 2\dfrac{n}{T_s}(\int_0^{T_s\times D_0} i_{Lr}(t)\cdot dt - \int_0^{\Delta D} i_{Lr}(t)\cdot dt) & (D = D_1) \\ I_{LV2} = 2\dfrac{n}{T_s}\int_0^{T_s\times D_2} i_{Lr}(t)\cdot dt \\ = 2\dfrac{n}{T_s}(\int_0^{T_s\times D_0} i_{Lr}(t)\cdot dt - \int_0^{\Delta D} i_{Lr}(t)\cdot dt) & (D = D_2) \\ I_{LV0} = 2\dfrac{n}{T_s}\int_0^{T_s\times D_0} i_{Lr}(t)\cdot dt & (D = D_0) \end{cases} \tag{15}$$

V_{LV} can be expressed as

$$V_{LV} = I_{LV}\cdot R_{LV} \tag{16}$$

V_{LV0} and ΔV can be defined as

$$\begin{cases} V_{LV0} = 2\dfrac{nR_{LV}}{T_s}\int_0^{T_s\times D_0} i_{Lr}(t)\cdot dt \\ \Delta V = 2\dfrac{nR_{LV}}{T_s}\int_0^{T_s\times \Delta D} i_{Lr}(t)\cdot dt \end{cases} \tag{17}$$

According (15), (16) and (17), when $D = D_0 \pm \Delta D$, V_{LV} can be simplified to $V_{LV} = V_{LV0} - \Delta V$. Based on the analysis of Section III(B), nV_{LV0}/V_{HV} is equal to 1, hence the voltage gain M can be expressed as

$$M = \frac{nV_{LV}}{V_{HV}} = 1 - \frac{n\Delta V}{V_{HV}} \tag{18}$$

It can be seen that when $D \neq D_0$, the average value of resonant current decreases, and it will cause the voltage gain to decrease and be less than 1. Meanwhile, when the converter operates at a non-optimal duty cycle (D_0), the circulating current and turn-off loss may be generated as shown in Fig.11(a) and Fig.11(b), so the efficiency of the converter will decrease. Hence the duty cycle needs to be adjusted in time to reach optimum point.

When the converter works, it always exists one optimal duty cycle ($D_0 = T_r/2T_s$) to make the voltage gain to be closest to 1. In order to unify the control logic of bidirectional power transmission, the unified voltage gain variation of forward and reverse power flows defined as

$$\begin{aligned} \Delta M &= \left|1 - \frac{nV_{LV}}{V_{HV}}\right| = \left|\frac{n\Delta V}{V_{HV}}\right| \\ &= \left|2\frac{n^2R_{LV}}{V_{HV}T_s}\int_0^{T_s\times\Delta D} i_{Lr}(t)\cdot dt\right| \end{aligned} \tag{19}$$

The relationship of ΔM and D is shown in Fig.12(a). It can be seen that there is only one optimal duty cycle to minimize the value of ΔM. According to this feature, the optimal duty cycle can be tracked by perturbation and observation method (P&O).

The control block diagram of the proposed control strategy is shown in Fig.12(b), the optimal duty cycle tracking by P&O does not need the current sense circuit, and it is realized by the input and output voltage sampling. In addition, the unified control strategy for bidirectional power flow simplifies the control complexity and improves the reliability.

The proposed control flowchart is shown in Fig.12(c) and it has three distinct stages as listed below:

1) Calculate ΔM according to (19).
2) Compare ΔM and D of this control cycle with the previous one.
3) If $\Delta M_n \geq \Delta M_{n-1}$ and $D_n \geq D_{n-1}$, the duty cycle needs to be adjusted to $D_{n+1} = D_n - \Delta D$; if $\Delta M_n \geq \Delta M_{n-1}$ and $D_n < D_{n-1}$, the duty cycle needs to be adjusted to $D_{n+1} = D_n + \Delta D$; if $\Delta M_n < \Delta M_{n-1}$ and $D_n \geq D_{n-1}$, the duty cycle needs to be adjusted to $D_{n+1} = D_n + \Delta D$; if $\Delta M_n < \Delta M_{n-1}$ and $D_n < D_{n-1}$, the duty cycle needs to be adjusted to $D_{n+1} = D_n - \Delta D$.

Repeat the above steps, and the converter will work at the optimal duty cycle to achieve a voltage gain which is closest to 1.

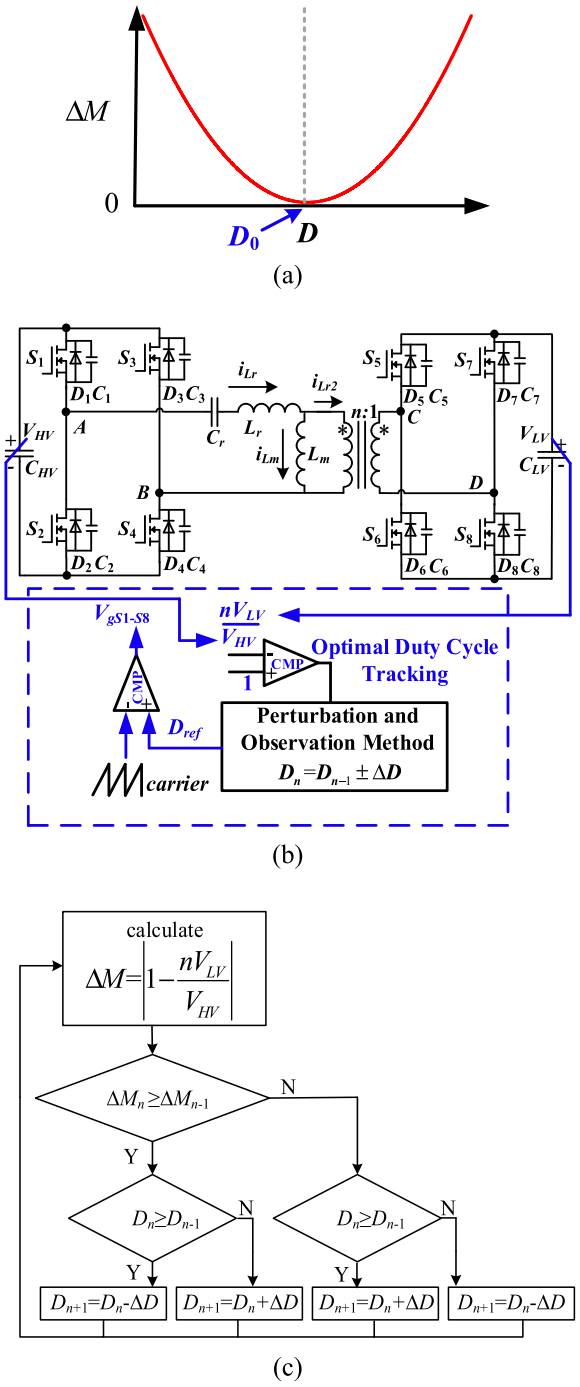

FIGURE 12. Control strategy. (a) Relationship of ΔM and D, (b) Control block diagram of the optimal duty cycle tracking, (c) Control flowchart of P&O to track optimal duty cycle.

The search step ΔD can be defined as

$$\Delta D = k(\Delta M_n - \Delta M_{n-1}) \tag{20}$$

where k is a non-negative constant.

According Fig.12(a) and (20), ΔM varies rapidly when it is away from the optimal duty cycle, hence the tracking step is long and the tracking speed is fast; when the duty cycle is approaching at the optimal point, ΔM varies slowly,

hence the tracking step size decreases and tends to zero. Finally, the converter works stably at the optimal duty cycle, meanwhile the steady-state errors and the oscillation are suppressed. In addition, when the heating or aging of the passive components causes the change of parameters, the converter can continue to track the optimal duty cycle after change.

V. DESIGN CONSIDERATIONS

This section introduces a design example of the proposed solutions with 340 V for HV and 20V for LV. The rated power is 1200W.

A. TURNS RATIO OF THE TRANSFORMER

According to (11), the voltage gain of the proposed modulation is 1, so the transformer turns ratio n can be derived as

$$\begin{aligned} \frac{nV_{LV}}{V_{HV}} &= 1 \\ &\Rightarrow n = V_{HV}/V_{LV} \end{aligned} \tag{21}$$

According to the range of designed transmission voltage. The turns ratio n is selected as 17.

B. RESONANT TANK, SWITCHING FREQUENCY AND TRACKING PARAMETERS

In order to ensure that the optimal resonant frequency can be tracked when the resonant parameter fluctuates by 30%. The dead time T_{DT} can be defined as

$$T_{DT} \approx 0.3 \cdot T_r \tag{22}$$

Hence the switching period and the switching frequency can be expressed as

$$\begin{cases} T_s \approx 1.3 \cdot T_r \\ f_s \approx \dfrac{10}{13} \cdot f_r \end{cases} \tag{23}$$

In addition, as seen from the boundary condition of DCM-CCM, $C_r > P/8f_sV_{HV}^2$ needs to be considered to ensure that the converter operates in DCM. Meanwhile $Z_r = \sqrt{L_r/C_r}$ needs to be high enough to reduce the peak value of the resonant current.

Because the tracking of the optimal duty cycle is aimed at the heating or aging of the devices which is under large time scale, the response speed does not need to be fast. In order to improve the stability of the system, the tracking period is set to millisecond level.

According to the above conditions, the design parameters are shown as following: $f_s = 60$kHz, $f_r = 86$kHz, $C_r = 0.1\mu$F, $L_r = 34\mu$H, the tracking period is 500ms and the initial tracking step is 0.2μs.

C. THE CONDITIONS OF SOFT SWITCHING

The excitation inductance should be selected to be as large as possible to reduce the circuiting current-related conduction loss. Also, the magnetizing inductance should be designed smaller enough to achieve ZVS. I_{Lm_pk} is the peak value of the excitation current which can be obtained by

$$I_{Lm_pk} = \frac{nV_{LV}}{4L_mf_s} = \frac{V_{HV}}{4L_mf_s} \tag{24}$$

The ZVS conditions of the HV-side MOSFETs and the LV-side MOSFETs can be obtained by

$$\begin{cases} \int_0^{T_{DT}} i_{L_m}(t) \geq 2V_{HV}C_{oss_HV} \\ n\int_0^{T_{DT}} i_{L_m}(t) \geq 2V_{LV}C_{oss_LV} \\ I_{Lm_pk} \geq \dfrac{nV_{LV}}{L_m}T_{DT} \end{cases} \tag{25}$$

According to (19) and (20), the boundary conditions of soft switching can be obtained

$$\begin{cases} L_m \leq \dfrac{T_{DT}}{8C_{oss_HV}}(T_S - 2T_{DT}) \\ \dfrac{L_m}{n^2} \leq \dfrac{T_{DT}}{8C_{oss_LV}}(T_S - 2T_{DT}) \\ T_{DT} \leq T_s/4 \end{cases} \tag{26}$$

In this paper, the type of HV side switches is FCH072N60F and the type of LV side switches is PSMN1R5-40PS. C_{OSS} of HV side switches is 441pF, C_{OSS} of LV side switches is 2042pF. According to the above equations, the magnetizing inductance L_m is chosen as 1.7mH, and the dead-time T_{DT} is from 0.7μs to 4μs.

VI. EXPERIMENTAL VERIFICATION

A 1200W experimental prototype is built to verify the effectiveness of the proposed solution. The application of the experimental prototype is the front-stage converter of two-stage topology. HVDC Bus is 340V which can connect to grid by inverter. LVDC Bus is 20V which can connect a bidirectional non-isolated DC-DC converter to regulate the voltage accurately. The experimental prototype designed in this paper can be regarded as a 340V/20V DC transformer. The specifications of the prototype are given in TABLE 1, based on the aforementioned design process.

TABLE 1. Parameters of the experimental prototype.

Designed parameters	Value
HVDC Bus (V_{HV})	340V
LVDC Bus (V_{LV})	20V
Rated power (P)	1200W
Turns ratio (n)	17
Resonant capacitor (C_r)	100nF
Resonant inductor (L_r)	34μH
Magnetizing inductor (L_m)	1.7mH
Resonant frequency (f_r)/Switching frequency (f_s)	86kHz/60kHz
HV side switches (S_1-S_4)	FCH072N60F
LV side switches (S_5-S_8)	PSMN1R5-40PS

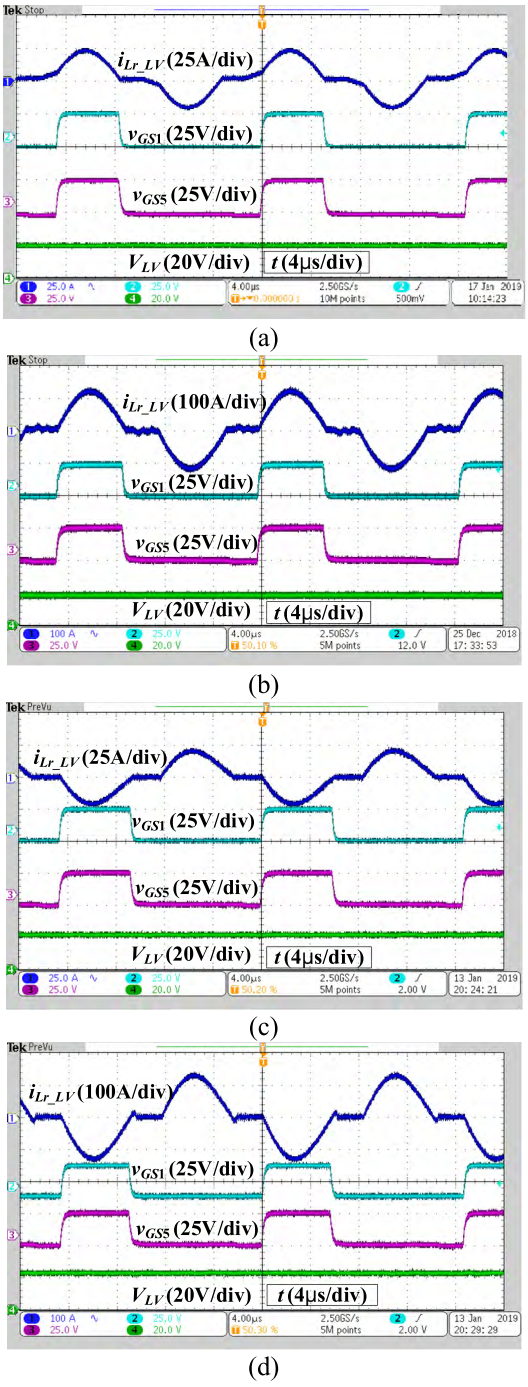

FIGURE 13. Steady-state waveforms with the optimal duty cycle tracking, (a) light load of forward transmission (200W), (b) full load of forward transmission (1200W), (c) light load of backward transmission (200W), (d) full load of backward transmission (1200W).

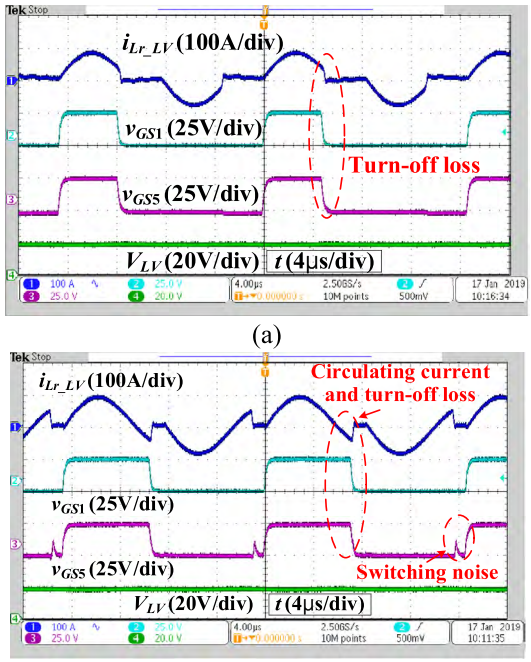

FIGURE 14. Waveforms of mismatched resonant parameters and duty cycle, (a) $D < D_0$, (b) $D > D_0$.

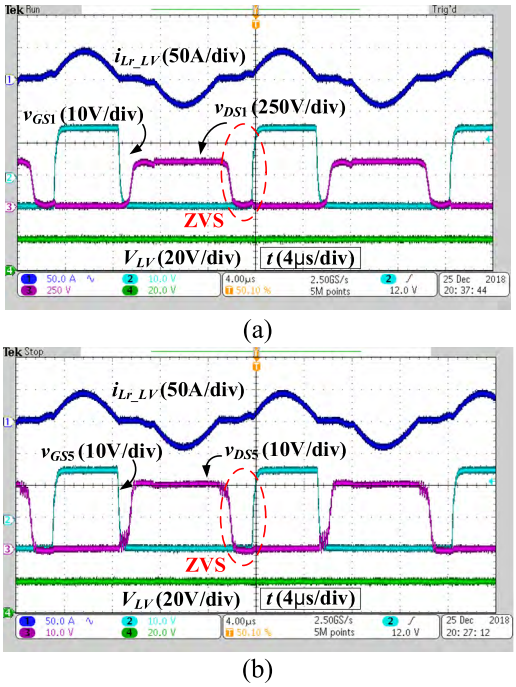

FIGURE 15. Soft-switching waveforms, (a) HV side switches ($S_1 - S_4$), (b) LV side switches ($S_5 - S_8$).

The waveforms when the resonant parameters are not matched with duty cycle without using proposed optimal duty cycle tracking method are shown in Fig.13. Fig.13(a) is the waveforms with $D < D_0 = T_r/2T_s$, and it can be seen that the switching signal turns off before the current reaches zero and the turn-off loss is generated. Fig.13(b) is the waveforms with $D > D_0 = \mathrm{T}_r/2\mathrm{T}_s$, and the circulating current, turn-off current and switching noise are existed. Therefore, the loss of the converter increases in these two cases.

The steady-state waveforms with the optimal duty cycle tracking are shown in Fig.14. Fig.14(a) and Fig.14(b) are the forward transmission waveforms of light load (200W) and full load (1200W), respectively. Fig.14(c) and Fig.14(d) are the backward transmission waveforms of light load (200W)

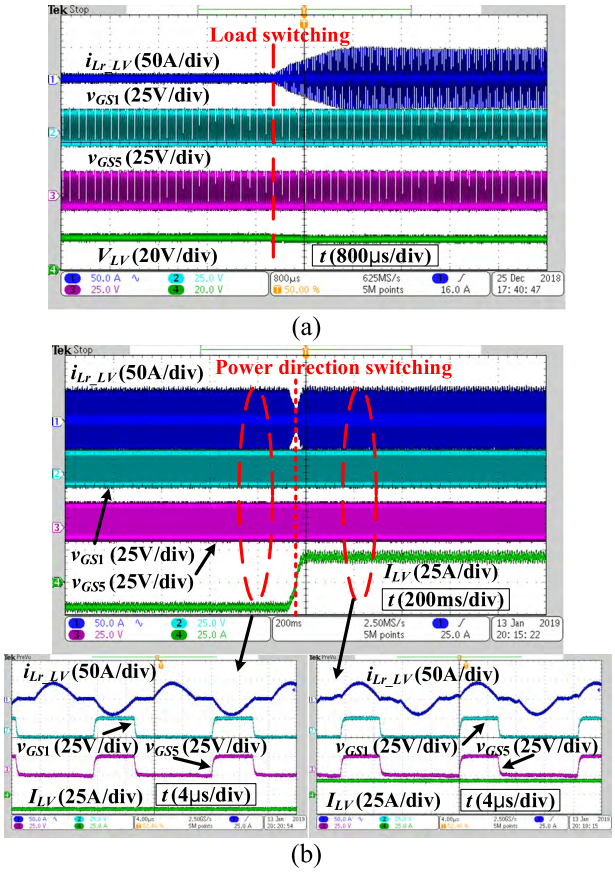

FIGURE 16. Dynamic waveforms, (a) no-load switching to forward 400W, (b) backward 400W switching to forward 400W.

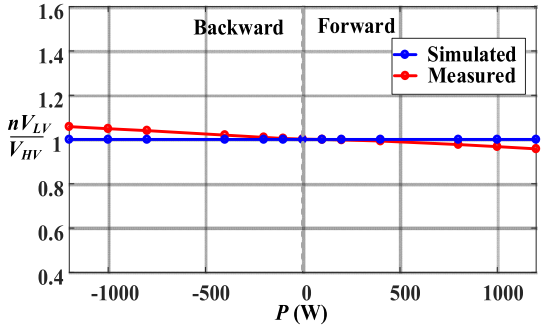

FIGURE 17. Voltage gain curves of the optimal duty cycle.

and full load (1200W). When the optimal duty cycle is tracked, the zero-crossing point of resonant current is fixed and does not change with load. Meanwhile, the waveforms of forward and backward power transmission are basically symmetrical and the driving signals for S_1 and S_5 are identical, which matches with the modulation scheme shown in Fig.6.

The soft switching waveforms are shown in Fig.15. It can be seen that ZVS can be achieved with the proposed modulation under bidirectional power transmission.

The dynamic waveforms are shown in Fig.16. Fig.16(a) is the waveforms of no-load switching to forward 400W. Fig.16(b) is the waveforms of backward 400W switching to forward 400W. As shown in Fig.16(a), when the load changes, the output voltage can be kept constant. As shown in Fig.16(b), the resonant current I_{Lr_LV} and the LV side currentI_{LV} change smoothly when the load and power direction switch. The experimental results show that the LLC converter achieves natural bidirectional power flow under the proposed modulation and control strategy.

The voltage gain curves of the optimal duty cycle are shown in Fig.17. The measured results are the actual values including the voltage drop of switches conduction and line conduction. It can be seen that the measured voltage gain is close to 1 under different load condition which is consistent with the simulation results.

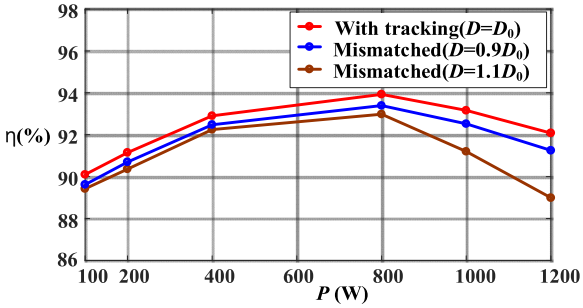

FIGURE 18. Measured efficiency cures of different duty cycle.

The efficiency curves of the proposed modulation are shown in Fig.18. Compared with the result of the mismatched resonant parameters, the converter has the highest efficiency with the optimal duty cycle tracking and the efficiency gap increases with the power.

VII. CONCLUSION

In this paper, a PWM modulation is presented to achieve naturally bidirectional power flow and synchronous rectification without adding auxiliary circuit for LLC-DCX When the resonant parameters changes, the converter performance can still be ensured with the proposed optimal duty cycle tracking method. It can maximize the system efficiency, provide fixed voltage ratio and locate the zero-crossing point of resonant current automatically. The working modes of the converter, DCM operating conditions and realization of duty cycle tracking are introduced in details. Experimental results have shown that the proposed method is effective to achieve naturally bidirectional power, constant gain and self-adaption for resonant parameter changing.

REFERENCES

[1] M. N. Kheraluwala, R. W. Gascoigne, D. M. Divan, and E. D. Baumann, "Performance characterization of a high-power dual active bridge DC-to-DC converter," *IEEE Trans. Ind. Appl.*, vol. 28, no. 6, pp. 1294–1301, Nov./Dec. 1992.

[2] G. Xu, D. Sha, J. Zhang, and X. Liao, "Unified boundary trapezoidal modulation control utilizing fixed duty cycle compensation and magnetizing current design for dual active bridge DC-DC converter," *IEEE Trans. Power Electron.*, vol. 32, no. 3, pp. 2243–2252, Mar. 2017.

[3] H. V. Nguyen, D.-D. To, and D.-C. Lee, "Onboard battery chargers for plug-in electric vehicles with dual functional circuit for low-voltage battery charging and active power decoupling," *IEEE Access*, vol. 6, pp. 70212–70222, 2018.

[4] G. Ma, W. Qu, G. Yu, Y. Liu, N. Liang, and W. Li, "A zero-voltage-switching bidirectional DC-DC converter with state analysis and soft-switching-oriented design consideration," *IEEE Trans. Ind. Electron.*, vol. 56, no. 6, pp. 2174–2184, Jun. 2009.
[5] X. Liu *et al.*, "Novel dual-phase-shift control with bidirectional inner phase shifts for a dual-active-bridge converter having low surge current and stable power control," *IEEE Trans. Power Electron.*, vol. 32, no. 5, pp. 4095–4106, May 2017.
[6] H. Shi *et al.*, "Minimum-backflow-power scheme of DAB-based solid-state transformer with extended-phase-shift control," *IEEE Trans. Ind. Appl.*, vol. 54, no. 4, pp. 3483–3496, Jul./Aug. 2018.
[7] D. Sha, X. Wang, K. Liu, and C. Chen, "A current-fed dual-active-bridge DC-DC converter using extended duty cycle control and magnetic-integrated inductors with optimized voltage mismatching control," *IEEE Trans. Power Electron.*, vol. 34, no. 1, pp. 462–473, Jan. 2019.
[8] D. Huang, F. C. Lee, and D. Fu, "Classification and selection methodology for multi-element resonant converters," in *Proc. IEEE 26th Annu. Appl. Power Electron. Conf. Expo.*, Mar. 2011, pp. 558–565.
[9] D. Huang, S. Ji, and F. C. Lee, "LLC resonant converter with matrix transformer," *IEEE Trans. Power Electron.*, vol. 29, no. 8, pp. 4339–4347, Aug. 2014.
[10] T. Sun, X. Ren, Q. Chen, Z. Zhang, and X. Ruan, "Reliability and efficiency improvement in LLC resonant converter by adopting GaN transistor," in *Proc. IEEE Appl. Power Electron. Conf. Expo. (APEC)*, Mar. 2015, pp. 2459–2463.
[11] T. Liu, Z. Zhou, A. Xiong, J. Zeng, and J. Ying, "A novel precise design method for LLC series resonant converter," in *Proc. 28th Int. Telecommun. Conf.*, Sep. 2006, pp. 1–6.
[12] X. Wu, H. Chen, and Z. Qian, "1-MHz LLC resonant DC transformer (DCX) with regulating capability," *IEEE Trans. Ind. Electron.*, vol. 63, no. 5, pp. 2904–2912, May 2016.
[13] H. Xu, Z. Yin, Y. Zhao, and Y. Huang, "Accurate design of high-efficiency LLC resonant converter with wide output voltage," *IEEE Access*, vol. 5, pp. 26653–26665, 2017.
[14] Z. Hu, Y. Qiu, Y. F. Liu, and P. C. Sen, "A control strategy and design method for interleaved LLC converters operating at variable switching frequency," *IEEE Trans. Power Electron.*, vol. 29, no. 8, pp. 4426–4437, Aug. 2014.
[15] D. F. D. Tan, "A review of immediate bus architecture: A system perspective," *IEEE J. Emerg. Sel. Topics Power Electron.*, vol. 2, no. 3, pp. 363–373, Sep. 2014.
[16] S. Lim, J. Ranson, D. M. Otten, and D. J. Perreault, "Two-stage power conversion architecture suitable for wide range input voltage," *IEEE Trans. Power Electron.*, vol. 30, no. 2, pp. 805–816, Feb. 2015.
[17] J.-Y. Lee, Y.-S. Jeong, H.-J. Chae, K.-M. Yoo, J.-J. Chang, and J.-H. Chang, "Two-stage insulated bidirectional DC/DC power converter using a constant duty ratio LLC resonant converter," U.S. Patent 20 110 090 717 A1, Apr. 21, 2011.
[18] D.-J. Gu, Z. Zhang, Y. Wu, D. Wang, H. Gui, and L. Wang, "High efficiency LLC DCX battery chargers with sinusoidal power decoupling control," in *Proc. IEEE Energy Convers. Congr. Expo. (ECCE)*, Sep. 2016, pp. 1–7.
[19] R. Ren, S. Liu, J. Wang, and F. H. Zhang, "High frequency LLC DC-transformer based on GaN devices and the dead time optimization," in *Proc. Int. Power Electron. Appl. Conf. Expo.*, Nov. 2014, pp. 462–467.
[20] B. Yang, F. C. Lee, A. J. Zhang, and G. Huang, "LLC resonant converter for front end DC/DC conversion," in *Proc. IEEE 7th Annu. Appl. Power Electron. Conf. Expo.*, Mar. 2002, pp. 1108–1112.
[21] X. Wu, G. Hua, J. Zhang, and Z. Qian, "A new current-driven synchronous rectifier for series-parallel resonant (LLC) DC-DC converter," *IEEE Trans. Ind. Electron.*, vol. 58, no. 1, pp. 289–297, Jan. 2011.
[22] W. Feng, F. C. Lee, P. Mattavelli, and D. Huang, "A universal adaptive driving scheme for synchronous rectification in LLC resonant converters," *IEEE Trans. Power Electron.*, vol. 27, no. 8, pp. 3775–3781, Aug. 2012.
[23] C. Fei, Q. Li, and F. C. Lee, "Digital implementation of adaptive synchronous rectifier (SR) driving scheme for high-frequency LLC converters with microcontroller," *IEEE Trans. Power Electron.*, vol. 33, no. 6, pp. 5361–5531, Jun. 2018.
[24] S. Abe *et al.*, "Sensing-less drive of synchronous rectifier for LLC resonant converter," in *Proc. Intelec*, Oct. 2012, pp. 1–6.
[25] J. Wang and B. Lu, "Open loop synchronous rectifier driver for LLC resonant converter," in *Proc. IEEE 28th Annu. Appl. Power Electron. Conf. Expo.*, Mar. 2013, pp. 2048–2051.
[26] T. Jiang, J. Zhang, X. Wu, K. Sheng, and Y. Wang, "A bidirectional LLC resonant converter with automatic forward and backward mode transition," *IEEE Trans. Power Electron.*, vol. 30, no. 2, pp. 757–770, Feb. 2015.
[27] W. Chen, P. Rong, and Z. Lu, "Snubberless bidirectional DC-DC converter with new CLLC resonant tank featuring minimized switching loss," *IEEE Trans. Ind. Electron.*, vol. 57, no. 9, pp. 3075–3086, Sep. 2010.
[28] K. Tan, R. Yu, S. Guo, and A. Q. Huang, "Optimal design methodology of bidirectional LLC resonant DC/DC converter for solid state transformer application," in *Proc. 40th IEEE Annu. Conf. Ind. Electron. Soc.*, Nov. 2014, pp. 1657–1664.
[29] X. Yu and P. Yeaman, "A new high efficiency isolated bi-directional DC-DC converter for DC-bus and battery-bank interface," in *Proc. IEEE Appl. Power Electron. Conf. Expo.*, Mar. 2014, pp. 879–883.
[30] A. Sankar, A. Mallik, and A. Khaligh, "Extended harmonics based phase tracking for synchronous rectification in CLLC converters," *IEEE Trans. Ind. Electron.*, vol. 66, no. 8, pp. 6592–6603, Aug. 2019.
[31] W. Feng, P. Mattavelli, and F. C. Lee, "Pulsewidth locked loop (PWLL) for automatic resonant frequency tracking in LLC DC-DC transformer (LLC-DCX)," *IEEE Trans. Power Electron.*, vol. 28, no. 4, pp. 1862–1869, Apr. 2013.
[32] H. Wang, S. Dusmez, and A. Khaligh, "Maximum efficiency point tracking technique for LLC-based PEV chargers through variable DC link control," *IEEE Trans. Ind. Electron.*, vol. 61, no. 11, pp. 6041–6049, Nov. 2014.
[33] M. Mohammadi and M. Ordonez, "Synchronous rectification of LLC resonant converters using homopolarity cycle modulation," *IEEE Trans. Ind. Electron.*, vol. 66, no. 3, pp. 1781–1790, Mar. 2019.
[34] S. Zong, G. Fan, and X. Yang, "Double voltage rectification modulation for bidirectional DC/DC resonant converters for wide voltage range operation," *IEEE Trans. Power Electron.*. to be published.
[35] J. Zhang, J. Liao, J. Wang, and Z. Qian, "A current-driving synchronous rectifier for an LLC resonant converter with voltage-doubler rectifier structure," *IEEE Trans. Power Electron.*, vol. 27, no. 4, pp. 1894–1904, Apr. 2012.

JINGTAO XU was born in Hubei, China, in 1994. He received the B.S. degree in electrical engineering and automation from Central South University, Changsha, China, in 2016, where he is currently pursuing the M.S. degree in electrical engineering. His research interests include modeling and control of power electronics converters.

JIAN YANG (M'09) received the Ph.D. degree in electrical engineering from the University of Central Florida, Orlando, FL, USA, in 2008. He was a Senior Electrical Engineer with Delta Tau Data Systems, Inc., Los Angeles, CA, USA, from 2007 to 2010. Since 2011, he has been with Central South University, Changsha, China, where he is currently a Professor with the School of Information Science and Engineering. His main research interests include motion control, power electronics and its applications in wind energy generation systems, and photovoltaic systems.

GUO XU (M'15) received the B.S. degree in electrical engineering and automation and the Ph.D. degree from the Beijing Institute of Technology, Beijing, China, in 2012 and 2018, respectively. From 2016 to 2017, he was a Visiting Student with the Center for Power Electronics System (CPES), Virginia Polytechnic Institute and State University, Blacksburg, VA, USA. Since 2018, he has been with the School of Information Science and Engineering, Central South University, Changsha, China, where he is currently an Associate Professor. His research interests include modeling and control of power electronics converters, high-efficiency power conversion, and magnetic integration in power converters.

TAOWEN JIANG was born in Hunan, China, in 1993. He received the B.Eng. degree in electrical engineering and automation from the Hunan University of Technology, Zhuzhou, China, in 2015. He is currently pursuing the M.E. degree in electrical engineering. His research interests include bidirectional DC-DC converter and renewable energy generation systems.

MEI SU was born in Hunan, China, in 1967. She received the B.S. degree in automation, and the M.S. and Ph.D. degrees in electric engineering from the School of Information Science and Engineering, Central South University, in 1989, 1992, and 2005, respectively, where she has been a Professor, since 2006. Her research interests include matrix converter, adjustable speed drives, and wind energy conversion systems.

YAO SUN (M'13) was born in Hunan, China, in 1981. He received the B.S., M.S., and Ph.D. degrees from the School of Information Science and Engineering, Central South University, Changsha, China, in 2004, 2007, and 2010, respectively, where he has been an Associate Professor, since 2013.

His research interests include matrix converter, micro-grid, and wind energy conversion systems.

HUI WANG received the B.S., M.S., and Ph.D. degrees from Central South University, Changsha, China, in 2008, 2011, and 2014, respectively, where he has been with the School of Information Science and Engineering, since 2016.

His research interests include matrix converter, DC/DC converters, and solid-state transformer.

MINGHUI ZHENG received the B.E. and M.E. degrees from Beihang University, Beijing, China, in 2008, 2011, and 2017, respectively, and the Ph.D. degree in mechanical engineering from the University of California at Berkeley, Berkeley, CA, USA. She joined the University at Buffalo, in 2017, where she is currently an Assistant Professor in mechanical and aerospace engineering. Her research interests include advanced learning, estimation, and control with applications to high-precision systems.